Lorentzian demodulation algorithm for multimode polymer optical fiber Bragg gratings

Yosuke Mizuno[1*], Tianyi Ma[1], Ryo Ishikawa[1], Heeyoung Lee[1], Antreas Theodosiou[2], Kyriacos Kalli[2], and Kentaro Nakamura[1]

1 Institute of Innovative Research, Tokyo Institute of Technology, Yokohama 226-8503, Japan
2 Photonics and Optical Sensing Research Laboratory, Cyprus University of Technology, Limassol 3036, Cyprus

[*]E-mail: ymizuno@sonic.pi.titech.ac.jp

Abstract: For strain sensing applications, we develop a simple and accurate Lorentzian demodulation algorithm for fiber Bragg gratings (FBGs) inscribed in multimode optical fibers. As multimode FBG spectra generally exhibit multiple peaks, simply tracking some particular spectral peaks (i.e., maximum detection) results in measurement failure when strain is large. Here, using an FBG inscribed in a perfluorinated graded-index multimode polymer optical fiber, we experimentally evaluate the new method by comparing its performance with those of other demodulation algorithms, such as maximum and centroid detection methods. Finally, using this method, we demonstrate the accurate measurement of strain of up to 1.0%.

Fiber Bragg gratings (FBGs) have been extensively studied because of their capability of highly accurate measurement of various physical parameters including strain, temperature, and humidity.[1–8)] Recently, FBGs have been inscribed not only in single-mode fibers (SMFs) but also in multimode fibers (MMFs).[9–11)] As MMF-FBG reflection spectra generally exhibit multiple peaks corresponding to different propagation modes, an accurate demodulation algorithm for detecting the Bragg wavelengths from multiple-peak FBG spectra is highly desirable.

MMFs in which FBGs can be inscribed include not only glass optical fibers but also polymer optical fibers (POFs).[12)] Owing to their high flexibility, POF-FBGs have been exploited to unique sensing applications.[13–15)] As well as in standard POFs composed of polymethyl methacrylate, FBGs have been successfully inscribed in perfluorinated graded-index (PFGI) POFs[16)] with relatively low loss at telecom wavelength by the use of a

femtosecond laser.[17,18] Although all the commercially available PFGI-POFs are MMFs, by exploiting some demodulation algorithms, they have already been used to develop various kinds of sensors.[19–21] Note that it is difficult and not practically convenient to excite a single peak (corresponding to the fundamental mode) in the PFGI-POF-FBGs.[22]

Of all the demodulation algorithms previously reported, what is the simplest is the maximum detection,[19,23] i.e., tracking a maximal peak (or some particular peaks). However, this method results in measurement failure when strain (or temperature change, etc.) is large, because, with increasing strain, the multiple peaks overlap with each other or get separated, as different peaks have different sensitivities. A centroid detection,[23] which is not largely influenced by such distortions of a single peak, has also been used, but it is largely affected by the background noise and the wavelength range used for demodulation. Cross-correlation,[23,24] which is also free from the influence of single-peak distortions, is a good way to solve these issue, but is reported to suffer from a so-called peak-locking effect.[25,26] To suppress this drawback, large amount of calculation time is required.[27] Recently, to further mitigate this shortcoming of the cross-correlation method, Theodosiou et al.[28] have developed an accurate, high-speed method by the combined use of cross-correlation and Hilbert transformation. Although this method can perform accurate detection of the Bragg wavelength with a short calculation time, the calculation process is relatively complicated and it has been applied only to relatively small strain of less than 0.1%.

In this work, we develop a simple and accurate demodulation algorithm based on Lorentzian approximation for detecting the Bragg wavelength of the multiple-peak FBG spectrum. Using a PFGI-POF-FBG sample, first, we show that the maximum and centroid detection methods lead to non-ideal results with insufficient accuracy. Then, we demonstrate the new demodulation method and prove its effectiveness by measuring relatively large strain of up to 1.0%.

As mentioned above, FBGs can be inscribed not only in SMFs but also in MMFs. Suppose a GI-MMF with a refractive index profile expressed as ($0 < r < R$):

$$n(r) = n_1 \sqrt{1 - 2\Delta \left(\frac{r}{R}\right)^g} \quad , \tag{1}$$

and ($R < r$):

$$n(r) = n_1 \sqrt{1 - 2\Delta} \quad , \tag{2}$$

where n_1 is the effective refractive index at the FBG reflection band, R is the core radius, Δ is the relative index difference between core and cladding, and g is the parabolic profile parameter. Then, the approximate number M of modes in the GI-MMF is given by:[29)]

$$M = \left(\frac{2\pi a}{\lambda} n_1\right)^2 \Delta \frac{g}{g+2} \quad , \tag{3}$$

where λ is the FBG reflection wavelength. If we substitute the parameters of a standard PFGI-POF (n_1 = 1.347, a = 25 um, Δ = ~0.01, g = 2, λ = ~1560 nm), the number of modes is estimated to be around 90 at this wavelength. When light is injected into this PFGI-POF (without any special control for exciting only the fundamental mode),[22)] some of these modes (especially, lower-order modes) are excited, generating multiple peaks at slightly different wavelengths in the FBG-reflected spectrum.

To detect the Bragg wavelength shift of the multiple-peak PFGI-POF-FBG spectrum, we propose a Lorentzian demodulation algorithm. The calculation procedures are schematically depicted in Fig. 1(a)–(d). Figure 1(a) shows an example of the target FBG-reflected spectrum with multiple peaks on a logarithm scale. As a first step, if necessary, this spectrum can be obtained using an optical spectrum analyzer (OSA) with a low frequency resolution (Fig. 1(b)). This is an optional step, which is sometimes beneficial when we use a low-cost OSA with a frequency resolution insufficient for accurate wavelength measurement of a single peak corresponding to a certain propagation mode. As a second step, we subtract the spectral noise floor of a light source from the measured spectrum (Fig. 1(c)). As a third step, we fit the spectrum with a Lorentzian curve:

$$L(\lambda) = \frac{A}{1 + \left(\frac{\lambda - \lambda_o}{W}\right)^2} \quad , \tag{4}$$

where A is the power of the spectral peak, λ_0 is the central wavelength, and W is the full width at half maximum, and derive its λ_0 value as the Bragg wavelength (Fig. 1(d)). These procedures are free from time-consuming and/or complicated calculations, and the sampling rate of the Bragg wavelength is solely determined by the sweeping frequency of the OSA. As experimentally shown later in this paper, this algorithm is almost free from the influence by distortions of some particular spectral peaks (as in the maximum detection) or by the spectral shape of the background noise and the wavelength range used for calculation (as in the centroid detection). Besides, this algorithm is not influenced by the peak-locking effect[25,26)] when the spectral position shifts in wavelength by less than the sampling

resolution of the OSA.

A 2-mm-long FBG was inscribed in a 1.4-m-long PFGI-POF.[16] The PFGI-POF (GigaPOF-50SR, Chromis Fiberoptics) has a three-layered structure: core (diameter: 50 μm; refractive index: ~1.35), cladding (diameter: 70 μm), and overcladding (diameter: 490 μm). The core and cladding are composed of doped and undoped amorphous fluoropolymer (CYTOP®), respectively, and the overcladding of polycarbonate. The optical propagation loss is relatively low (~0.25 dB/m) even at 1550 nm. The FBG was inscribed to the midpoint of the PFGI-POF without removal of the overcladding using a femtosecond laser system (High Q femtoREGEN) operating at 517 nm, with a pulse duration of 220 fs, a repetition rate of 1 kHz, and laser pulse energy of ~100 nJ. The PFGI-POF was mounted on an air bearing translation system for accurate two-axis motion and the laser beam was focused from above using a long working distance x50 objective. Accurate synchronization of the laser pulse repetition rate and stage motion allowed for plane-by-plane grating inscription, writing the grating to the desired length and index modulation value.

Figure 2 shows the experimental setup for observing the spectrum of the light reflected from the FBG inscribed in the PFGI-POF. The output from an amplified spontaneous emission (ASE) source was injected into the PFGI-POF, and the reflected light from the FBG was guided via an optical circulator to an OSA (AQ6370, Yokogawa). A 0.2-m-long section of the PFGI-POF including the FBG was strained using automatic translation stages. The room temperature was 25 °C.

Figure 3(a) shows the measured strain dependence of the FBG-reflected spectrum (corresponding to the 4th grating order)[21] when the resolution of the OSA was 0.02 nm (highest). Multiple peaks corresponding to different modes were observed. With increasing strain, the Bragg wavelength shifted to longer wavelength. To quantitatively evaluate the strain dependence of the Bragg wavelength, some demodulation techniques need to be employed.

Figure 3(b) shows the strain dependence of the Bragg wavelength when the maximum detection method was used, i.e., when the central wavelength of the spectral peak with the highest power was tracked. The dependence was almost linear, but the Bragg wavelength hopping was observed 4 times in this strain range. Consequently, four different coefficients were obtained depending on the strain range, one of them (~12.6 nm/%) was ~12 % different from the previously reported correct value (~14.3 nm/%).[13] This result originated from the overlap and/or separation of the spectral peaks when strain was applied. As the Bragg wavelength and the strain are not in one-to-one correspondence in this situation, the

maximum detection method was confirmed not to be directly available for strain sensing.

Figure 3(c) shows the strain dependence of the Bragg wavelength when the centroid detection method was used. When the centroids were calculated, the unit of the vertical axis was converted from dBm (log) into mW (linear). The spectral data in the wavelength range from 1550 to 1580 nm were used to calculate the centroids. The calculated Bragg wavelength dependence was far from being linear and was not even in one-to-one correspondence to strain, which indicates that the centroid detection method cannot be directly used for strain sensing. The nonlinear and non-monotonic dependence was clearly caused by the non-negligible noise floor. Namely, when strain was larger, the power of the FBG-reflected peaks became comparable to the noise floor, the contribution of which to the centroid became significant. This also explains the reason why the strain-induced wavelength shift of the centroid (< 5 nm) was much smaller than that of the spectral peak (> 13 nm). Thus, the centroid detection method was confirmed to be unsuitable for strain sensing unless the noise floor is negligibly flat. It is also clear that, with such a considerable noise floor, the result will be largely affected by the wavelength range used for calculation.

Subsequently, Figs. 4(a)–(c) show how the FBG-reflected spectrum was deformed at each step of the calculation procedures of the new method. As a first step, we measured the FBG-reflected spectrum intentionally with the lowest resolution [2.00 nm; Fig. 4(a)]; as mentioned above, this step is not necessary for the Lorentzian demodulation algorithm itself, but we intended to show the feasibility of employing a low-cost OSA with insufficient resolution. Here, as an example, the spectrum at strain of 0.5% was shown. The wavelength range needs to be adjusted depending on the maximal strain to be measured. As a second step, we subtracted the spectral noise floor of the ASE from the measured spectrum (Fig. 4(b)). As the third step, we fitted the spectrum with a Lorentzian curve (Fig. 4(c)) and derived its central wavelength as the Bragg wavelength (1564.2 nm).

We performed these procedures to Fig. 3(a) and obtained the strain dependence of the FBG-reflected spectrum, as shown in Fig. 5(a). Note that the vertical axis was normalized so that the peak power became 1. In the same manner as in Fig. 3(a), with increasing strain, the Bragg wavelength shifted to longer wavelength. Subsequently, we plotted the Bragg wavelength as a function of strain (Fig. 5(b)). The dependence was linear in the strain range of up to 1.0% with no wavelength hopping, and the calculated coefficient was ~14.1 nm/%, which is in good agreement with the previously reported value (~14.3 nm/%).[13)] Note that the bandwidth of the Lorentzian curve did not exhibit monotonic dependence on

strain (Fig. 5(a)), because each peak included in the spectrum shifts with its independent strain coefficient. This means that it is difficult to use the Bragg wavelength and the bandwidth simultaneously to perform discriminative measurement of two physical parameters, such as strain and temperature.

In conclusion, we developed a simple and accurate demodulation algorithm based on Lorentzian approximation for detecting the Bragg wavelength of the multiple-peak FBG spectrum. First, the maximum and centroid detection methods were shown to lead to measurement failure, especially when strain was larger (> 0.3%). Subsequently, the correct Bragg wavelength detection at strain of up to 1.0% was experimentally shown to be feasible using a PFGI-POF-FBG with our demodulation method. We anticipate that this method will be one of the standard tools for detecting the Bragg wavelength from a multiple-peak FBG (such as a POF-FBG) spectrum in the future.

Acknowledgments

This work was supported by JSPS KAKENHI Grant Numbers 17H04930 and 17J07226 and by a research grant from the Fujikura Foundation.

References

1) R. Kashyap, *Fiber Bragg Gratings* (Elsevier, San Diego, 1999).
2) A. Othonos and K. Kalli, *Fiber Bragg Gratings: Fundamentals and Applications in Telecommunications and Sensing* (Artech House, Boston, 1996).
3) P. Kronenberg, P. K. Rastogi, P. Giaccari, and H. G. Limberger, Opt. Lett. **27**, 1385 (2002).
4) M. G. Xu, L. Reekie, Y. T. Chow, and J. P. Dakin, Electron. Lett. **29** 398 (1993).
5) X. Sang, C. Yu, T. Mayteevarunyoo, K. Wang, Q. Zhang, and P. L. Chu, Sens. Actuators B: Chem. **120**, 754 (2007).
6) K. Krebber, H. Henschel, and U. Weinand, Meas. Sci. Technol. **17**, 1095 (2006).
7) Y. J. Eao, Meas. Sci. Technol. **8**, 355 (1997).
8) F. Farahi, D. J. Webb, J. D. C. Jones, and D. A. Jackson, J. Lightwave Technol. **8**, 138 (1990).
9) C. L. Zhao, X. Yang, M. S. Demokan, and W. Jin, J. Lightwave Technol. **24**, 879 (2006).
10) T. Mizunami, T. V. Djambova, T. Niiho, and S. Gupta, J. Lightwave Technol. **18**, 230 (2000).
11) Z. Yong, C. Zhan, J. Lee, S. Yin, and P. Ruffin, Opt. Lett. **31**, 1794 (2006).
12) M. G. Kuzyk, *Polymer Fiber Optics: Materials, Physics, and Applications* (CRC Press,

San Diego, 2006).
13) D. J. Webb, Mean. Sci. Technol. **26**, 092004 (2015).
14) Z. Xiong, G. D. Peng, B. Wu, and P. L. Chu, IEEE Photonics Technol. Lett. **11**, 352 (1999).
15) I. P. Johnson, K. Kalli, and D. J. Webb, Electron. Lett. **46**, 1217 (2010).
16) Y. Koike and M. Asai, NPG Asia Mater. **1**, 22 (2009).
17) A. Lacraz, M. Polis, A. Theodosiou, C. Koutsides, and K. Kalli, IEEE Photonics Technol. Lett. **27**, 693 (2015).
18) M. Koerdt, S. Kibben, J, Hesselbach, C. Brauner, A. S. Herrmann, F. Vollertsen, and L. Kroll, Proc. Technol. **15**, 138 (2014).
19) R. Ishikawa, H. Lee, A. Lacraz, A. Theodosiou, K. Kalli, Y. Mizuno, and K. Nakamura, IEEE Photonics Technol. Lett. **29**, 2167 (2017).
20) P. Stajanca, A. Lacraz, K. Kalli, M. Schukar, and K. Krebber, Proc. SPIE **9899**, 989911 (2016).
21) R. Ishikawa, H. Lee, A. Lacraz, A. Theodosiou, K. Kalli, Y. Mizuno, and K. Nakamura, Jpn. J. Appl. Phys. **57**, 038002 (2018).
22) A. Theodosiou, A. Lacraz, A. Stassis, c. Koutsides, M. Komodromos, and K. Kalli, J. Lightwave Technol. **35**, 5404 (2017).
23) A. Lamberti, S. Vanlanduit, B. D. Pauw, and F. Berghmans, Sensors **14**, 24258 (2014).
24) C. Huang, W. Jing, K. Liu, Y. Zhang, and G. D. Peng, IEEE Photonics Technol. Lett. **19**, 707 (2007).
25) J. Westerweel, Meas. Sci. Technol. **8**, 1379 (1997).
26) L. Gui and S. T. Wereley, Exp. Fluids **32**, 506 (2002).
27) S. D. Dyer, P. A. Williams, R. J. Espejo, J. D. Kofler, and S. M. Etzel, Proc. SPIE **5855**, 88 (2005).
28) A. Theodosiou, M. Komodromos, and K. Kalli, J. Lightwave Technol. **35**, 3956 (2017).
29) T. L. Singal, *Optical Fiber Communications: Principles and Applications* (Cambridge University Press, Cambridge, 2017).

Figure Captions

Fig. 1. (Color online) Schematic calculation procedures of the new method for detecting the Bragg wavelength. (a) FBG-reflected spectrum measured with a high resolution (step 0). (b) Spectrum intentionally measured with an extremely low resolution (step 1; optional). (c) Spectrum with the noise floor subtracted (step 2). (d) Lorentzian-fitted spectrum, from which the Bragg wavelength is derived (step 3).

Fig. 2. (Color online) Schematic of the experimental setup. ASE: amplified spontaneous emission.

Fig. 3. (Color online) (a) Strain dependence of the FBG-reflected spectrum. (b) Strain dependence of the Bragg wavelength calculated using the maximum detection method. (c) Strain dependence of the Bragg wavelength calculated using the centroid detection method.

Fig. 4. (Color online) (a) FBG-reflected spectrum (when strain was 0.50 %) measured with the lowest resolution (2.00 nm) on the optical spectrum analyzer. (b) FBG-reflected spectrum from which the noise floor was subtracted. (c) Lorentzian-fitted FBG-reflected spectrum.

Fig. 5. (Color online) Strain dependencies of (a) the normalized FBG-reflected spectrum and (b) the Bragg wavelength calculated using the new method. The dotted line is a linear fit.

Figures

Fig. 1.

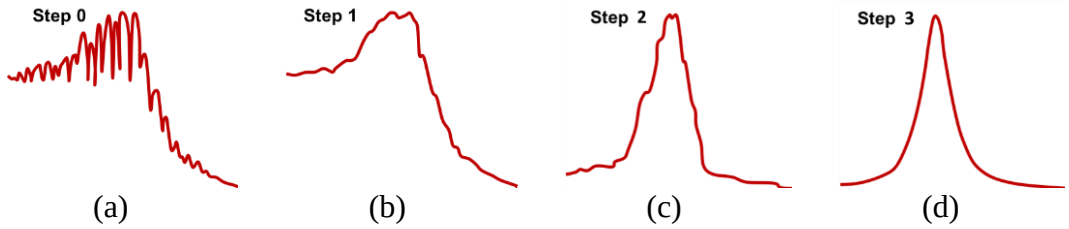

(a) (b) (c) (d)

Fig. 2.

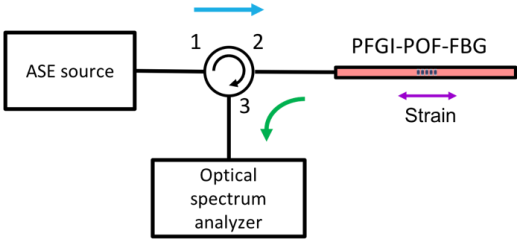

Fig. 3

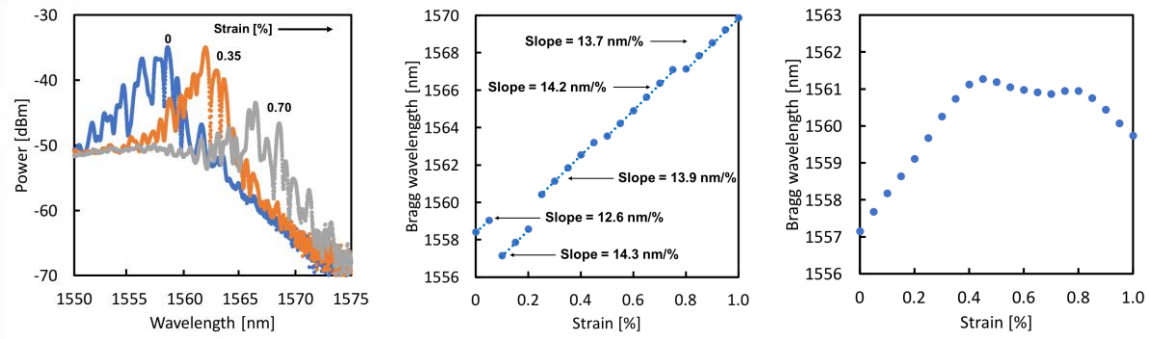

(a) (b) (c)

Fig. 4

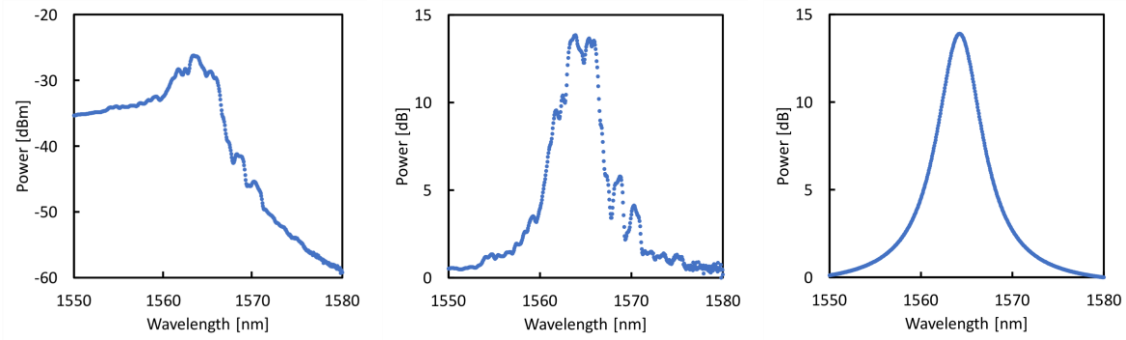

(a) (b) (c)

Fig. 5

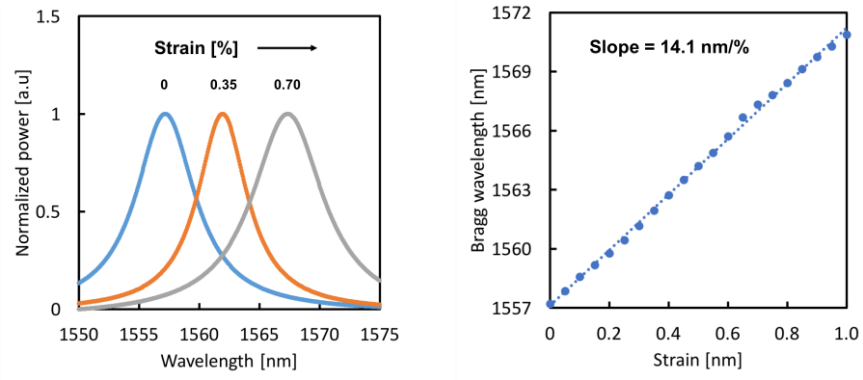
Strain [%]
0
0.35
0.70
Normalized power [a.u]
Wavelength [nm]
1.5
1
0.5
0
1550
1555
1560
1565
1570
1575
Slope = 14.1 nm/%
Bragg wavelength [nm]
Strain [nm]
1572
1569
1566
1563
1560
1557
0
0.2
0.4
0.6
0.8
1.0

(a) (b)